

AD-A103 102

COMPUTATION OF FLOW AROUND MANEUVERING SUBMERGED BODIES
(U) SCIENTIFIC RESEARCH ASSOCIATES INC GLASTONBURY CT
T R GOVINDAN ET AL. SEP 86 SRA-R86-920024-F

1/1

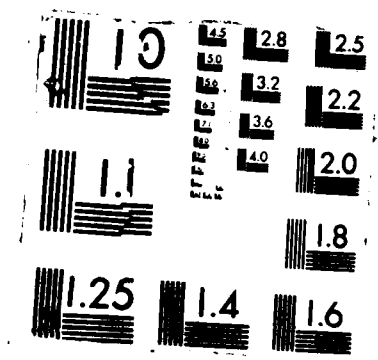
UNCLASSIFIED

N00014-85-C-0253

F/G 20/4

NL

					o					o	o	o	



AD-A183 102

DTIC FILE COPY

①

REPORT R86-920024-F
COMPUTATION OF FLOW AROUND MANEUVERING SUBMERGED BODIES

T.R. Govindan and R. Levy
Scientific Research Associates, Inc.
Glastonbury CT 06033

Final Report
Contract N00014-85-C-0253

Prepared for:
David W. Taylor Research and Development Center
Bethesda, Maryland 20084

September 1986

DTIC
S ELECTED D
JUL 31 1987
RD

DISTRIBUTION STATEMENT A
Approved for public release;
Distribution Unlimited

87 7 30 047

REPORT DOCUMENTATION PAGE

1a. REPORT SECURITY CLASSIFICATION UNCLASSIFIED		1b. RESTRICTIVE MARKINGS N/A	
2a. SECURITY CLASSIFICATION AUTHORITY N/A		3. DISTRIBUTION/AVAILABILITY OF REPORT APPROVED FOR PUBLIC RELEASE; DISTRIBUTION UNLIMITED	
2b. DECLASSIFICATION/DOWNGRADING SCHEDULE N/A		4. PERFORMING ORGANIZATION REPORT NUMBER(S) Report No. R86-920024-F	
4. PERFORMING ORGANIZATION REPORT NUMBER(S) Report No. R86-920024-F		5. MONITORING ORGANIZATION REPORT NUMBER(S)	
6a. NAME OF PERFORMING ORGANIZATION Scientific Research Asso., Inc	6b. OFFICE SYMBOL (if applicable)	7a. NAME OF MONITORING ORGANIZATION DAVID W. TAYLOR NAVAL SHIP RESEARCH AND DEVELOPMENT CENTER, Code 1504 (1505)	
6c. ADDRESS (City, State, and ZIP Code) P. O. Box 498 Glastonbury, CT 06033		7b. ADDRESS (City, State, and ZIP Code) BETHESDA, MARYLAND 20084-5000	
8a. NAME OF FUNDING/SPONSORING ORGANIZATION Naval Sea Systems Command	8b. OFFICE SYMBOL (if applicable) SEA 05R24	9. PROCUREMENT INSTRUMENT IDENTIFICATION NUMBER Contract Number - N00014-85-C-0253	
8c. ADDRESS (City, State, and ZIP Code) Washington, D. C. 20360		10. SOURCE OF FUNDING NUMBERS	
		PROGRAM ELEMENT NO 61153N	PROJECT NO SR 023 01
		TASK NO 23454	WORK UNIT ACCESSION NO N/A
11. TITLE (Include Security Classification) COMPUTATION OF FLOW AROUND MANEUVERING SUBMERGED BODIES			
12. PERSONAL AUTHOR(S) T. R. Govindan and R. Levy			
13a. TYPE OF REPORT Final	13b. TIME COVERED FROM 4/85 TO 3/86	14. DATE OF REPORT (Year, Month, Day) September 1986	15. PAGE COUNT 23
16. SUPPLEMENTARY NOTATION Sponsored under the Naval Sea Systems Command General Hydromechanics Research (GHR) Program administered by the David W. Taylor Naval Ship R&D Center, Code 1504 (1505), Bethesda, Maryland 20084-5000			
17. COSATI CODES		18. SUBJECT TERMS (Continue on reverse if necessary and identify by block number)	
FIELD	GROUP	SUB-GROUP	
20	04	(U) GHR Program (U) Submerged Bodies (U) Flow Field	
19. ABSTRACT (Continue on reverse if necessary and identify by block number) (U) The flow around submerged bodies at different attitudes evokes considerable interest in the field of hydrodynamics. Such flow fields occur in many and varied applications. Of particular interest is the flow field around a submarine, torpedo, or similar body in maneuver. The computation of this flow field is important to the analysis of performance and noise characteristics of the device.			
20. DISTRIBUTION/AVAILABILITY OF ABSTRACT <input checked="" type="checkbox"/> UNCLASSIFIED/UNLIMITED <input type="checkbox"/> SAME AS RPT <input type="checkbox"/> DTIC USERS		21. ABSTRACT SECURITY CLASSIFICATION UNCLASSIFIED	
22a. NAME OF RESPONSIBLE INDIVIDUAL Mr. V. J. Monacella		22b. TELEPHONE (Include Area Code) 202-227-1503	22c. OFFICE SYMBOL Code 1504/1505

cross-stream velocities, which may be an important element in the flow fields being considered here. Over the past few years, several investigators have suggested methods aimed at obtaining physically realistic and numerically sound forward marching procedures for three-dimensional viscous flows. In general, these methods utilize a three-dimensional viscous approach based on approximate governing equations which suppress streamwise elliptic effects requiring downstream boundary conditions. Motivated by these same goals, Briley and McDonald (Ref. 4) have developed a viscous primary/secondary flow analysis for the prediction of a wide class of subsonic flows at high Reynolds number in straight or smoothly curved flow geometries. This approach is applicable to flows which have a predominant primary flow direction with transverse secondary flow and synthesizes concepts from inviscid flow theory, secondary flow theory, and "extended" three-dimensional boundary layer theory. In Ref. 4, Briley and McDonald applied this analysis to three-dimensional flow in curved passages and predicted the development of the passage flow field including the formation and development of passage and corner vortices.

This approach has been applied at SRA to the problems of flow in circular ducts with curved centerlines (Ref. 5), lobe mixer flows (Ref. 6), further passage studies (Ref. 7), and to the tip vortex flow problem for a helicopter rotor blade (Ref. 8). Of particular interest here is the on-going effort at SRA for the computation of flow in the region of a hull-sail corner in submarines (Ref. 9) and the generation and development of the tip vortex in a ship propeller (Ref. 10). The effort has concentrated on the use of a forward marching procedure for the computation of flows over component parts of submarines, torpedoes and similar bodies. The effort here has been to extend the forward marching procedure to the computation of flows over submerged bodies that resemble submarine and torpedo body shapes at different attitudes. Several tasks were identified to comprise this effort. Progress made in completing these tasks is described in this report.

The next section of this report describes the forward marching procedure extended here to compute flow over submerged bodies. The third section describes tasks that have been completed and results obtained. The final section describes current on-going tasks, as well as future work required to extend the forward marching procedure to obtain quantitatively accurate predictions of the flow field over submerged bodies.

2. FORWARD MARCHING COMPUTATION PROCEDURE

The forward marching computation procedure for the solution of the parabolized Navier-Stokes equations provides an economical and accurate method for computing many three-dimensional viscous flow fields. The procedure, initially developed for internal flow fields, is being extended to the computation of flow over submerged bodies. The governing equations and computation scheme are presented in this section.

The governing equations are derived through approximations made relative to a curvilinear coordinate system fitted to and aligned with the flow geometry under consideration. The coordinate system is chosen such that the streamwise or marching coordinate either coincides with or is at least approximately aligned with a known inviscid primary flow direction as determined, for example, by a potential flow analysis for the given geometry. Transverse coordinate surfaces must be approximately perpendicular to solid walls or bounding surfaces, since diffusion is permitted only in these transverse coordinate surfaces.

Equations governing primary flow velocity U_p , and secondary vorticity, Ω_n , normal to transverse coordinate surfaces are derived utilizing approximations which permit solution of the governing equations as an initial-value problem, provided reversal of the composite streamwise velocity does not occur. Streamwise diffusion terms are neglected. Secondary flow velocities are determined from scalar and vector surface potential calculations on the transverse coordinate surfaces once the primary velocity and secondary vorticity are known.

Primary-Secondary Velocity Decomposition

In what follows, vectors are denoted by an overbar and unit vectors by a caret. The analysis is based on decomposition of the overall velocity vector field, \bar{U} , into a primary flow velocity, \bar{U}_p , and a secondary flow velocity, \bar{U}_s . The overall or composite velocity is determined from the superposition

$$\bar{U} = \bar{U}_p + \bar{U}_s \quad (1)$$

The primary flow velocity is represented as

$$\bar{U}_p = U_p \hat{i}_p \quad (2)$$

where \hat{i}_p is a known inviscid primary flow direction determined, for example, from an a priori potential flow solution for the geometry under consideration. A streamwise coordinate direction from a body fitted coordinate system could be used as an approximation to this potential flow direction. It should be noted that while accurate determination of the flow field requires prior specification of an inviscid pressure field, in this initial work the inviscid pressure has been assumed constant. Later phases of this work will include specification of an appropriate pressure field. The primary velocity, \bar{U}_p , is determined from the solution of a primary flow momentum equation. The secondary flow velocity, \bar{U}_s , is derived from scalar and vector surface potential, denoted ϕ and ψ , respectively. If \hat{i}_n denotes the unit vector normal to transverse coordinate surfaces, if ρ is density, and if ρ_0 is an arbitrary constant reference density, then \bar{U}_s is defined by

$$\bar{U}_s \equiv \nabla_s \phi + (\rho_0/\rho) \nabla x \hat{i}_n \psi \quad (3)$$

where ∇_s is the surface gradient operator defined by

$$\nabla_s \equiv \nabla - \hat{i}_n (\hat{i}_n \cdot \nabla) \quad (4)$$

It follows that since $\hat{i}_n \cdot \bar{U}_s = 0$, then \bar{U}_s lies entirely within transverse coordinate surfaces. Equation (3) is a general form permitting both rotational and irrotational secondary flows and will lead to governing equations which may be solved as an initial value problem. The overall velocity decomposition, Eq. (1), can be written

$$\bar{U} = U_p \hat{i}_p + \nabla_s \phi + (\rho_0/\rho) \nabla x \hat{i}_n \psi \quad (5)$$

Surface Potential Equations

Equations relating ϕ and ψ with U_p , ρ , and the secondary vorticity component, Ω_n , can be derived using Eq. (5) as follows. From continuity,

$$\nabla \cdot \rho \bar{U} = 0 = \nabla \cdot \rho U_p \hat{i}_p + \nabla \cdot \rho \nabla_S \phi + \rho_0 \nabla \cdot \nabla x \hat{i}_n \psi \quad (6)$$

and from the definition of the vorticity based on the secondary flow within the transverse surfaces, Ω_n

$$\hat{i}_n \cdot \nabla x \bar{U} \equiv \Omega_n \equiv \hat{i}_n \cdot \nabla x U_p \hat{i}_p + \hat{i}_n \cdot \nabla x (\rho_0 / \rho) \nabla x \hat{i}_n \psi + \hat{i}_n \cdot \nabla x \nabla_S \phi$$

Since the last term in each of Eqs. (6) and (7) is zero by vector identity, Eqs. (6) and (7) can be written as

$$\nabla \cdot \rho \nabla_S \phi = -\nabla \cdot \rho U_p \hat{i}_p \quad (8)$$

$$\hat{i}_n \cdot \nabla x (\rho_0 / \rho) \nabla x \hat{i}_n \psi = \Omega_n - \hat{i}_n \cdot \nabla x U_p \hat{i}_p \quad (9)$$

Note that the last term in Eq. (9) is identically zero in a coordinate system for which \hat{i}_n and \hat{i}_p have the same direction, and would be small if \hat{i}_n and \hat{i}_p are approximately aligned. In any event, given a knowledge of U_p , Ω_n and ρ , the surface potentials, ϕ and ψ , can be determined by a two-dimensional elliptic calculation in transverse coordinate surfaces at each streamwise location. In turn, \bar{U}_S can be computed from Eq. (3), and the composite velocity, \bar{U} , will satisfy continuity. Equations for U_p and Ω_n are obtained from the equations governing momentum and vorticity, respectively.

The streamwise momentum equation is given by

$$\hat{i}_p \cdot [(U \cdot \nabla)U + (\nabla P) / \rho] = \hat{i}_p \cdot \bar{F} + \hat{i}_p \cdot \bar{R} \quad (10)$$

where P is pressure and $\rho \bar{F}$ is force due to viscous stress and terms in \bar{R} representing streamwise diffusion are neglected. The pressure term in the streamwise momentum equation (10) can be taken from a simpler analysis such as a potential flow analysis. While this results in a set of equations which can be solved by forward marching, the surface pressures which are due to the pressure field imposed upon the flow are the potential flow pressures. Since the actual surface pressures are often of primary interest, a new estimate of the actual surface pressure which includes viscous and secondary flow effects can be computed from the resulting velocity field in the following manner.

The momentum equations in the transverse surfaces are:

$$\begin{aligned}\hat{i}_1 \cdot [(\rho \bar{U} \cdot \nabla) \bar{U} + \nabla P - \rho \bar{F} - \rho \bar{R}] &= 0 \\ \hat{i}_2 \cdot [(\rho \bar{U} \cdot \nabla) \bar{U} + \nabla P - \rho \bar{F} - \rho \bar{R}] &= 0\end{aligned}\quad (11)$$

Equation (11) represents components of the momentum vector in the transverse surfaces:

$$\hat{i}_1 (\hat{i}_1 \cdot [(\rho \bar{U} \cdot \nabla) \bar{U} + \nabla P - \rho \bar{F} - \rho \bar{R}]) + \hat{i}_2 (\hat{i}_2 \cdot [(\rho \bar{U} \cdot \nabla) \bar{U} + \nabla P - \rho \bar{F} - \rho \bar{R}]) \quad (12)$$

The divergence of this vector can be written as a Poisson equation for the pressure, P, at each transverse surface:

$$\begin{aligned}\nabla_S^2 P = \nabla^2 (P_I + P_C) &= - \frac{\partial}{\partial x_1} (\hat{i}_1 \cdot [(\rho \bar{U} \cdot \nabla) \bar{U} - \rho \bar{F} - \rho \bar{R}]) \\ &- \frac{\partial}{\partial x_2} (\hat{i}_2 \cdot [(\rho \bar{U} \cdot \nabla) \bar{U} - \rho \bar{F} - \rho \bar{R}])\end{aligned}\quad (13)$$

where P_I is the imposed pressure, P_C is a viscous correction to the pressure field and x_1 and x_2 are coordinates in the \hat{i}_1 and \hat{i}_2 directions, respectively. Equation (13) can be solved for the pressure correction, P_C , at each computational station using Neuman boundary conditions derived from Eq. (12). The use of Neuman boundary conditions requires an additional parameter which is only a function of the normal direction, $P_v(x_3)$, in order to set the level of the pressure field. For external flows, $P_v(x_3)$ is set to match the imposed pressure at an appropriate far field location.

Secondary Vorticity

The equation governing Ω_n is obtained by cross differentiating each of the transverse momentum equations (11). Eliminating the pressure in the two equations results in a single equation for the transport of the vorticity normal to the transverse surface. This equation has the form

$$\bar{U} \cdot \nabla \Omega_n - \bar{\Omega} \cdot \nabla U_n = G_n + C + \hat{i}_n \cdot (\nabla \times \bar{R}) \quad (14)$$

where G_n is the normal component of

$$\bar{G} = \nabla \times \bar{F} \quad (14)$$

and C is a collection of curvature terms arising from changes in orientation of the transverse surfaces as a function of streamwise coordinate.

System of Governing Equations

A complete system of four coupled equations governing U_p , Ω_n , ϕ and ψ is given by Eqs. (8), (9), (10) and (14). Ancillary relations are given by Eq. (5) for composite velocity, and Eq. (13) for pressure.

Numerical Method

Since techniques for obtaining the basic potential flow solution are well known and numerous, they need not be enumerated or discussed here. Instead, the present development concentrates on describing the numerical method used to solve the system of governing equations. Streamwise derivative terms in the governing equations have a form such as $u_1 \partial(\) / \partial x_1$, and because the streamwise velocity, u_1 , is very small in the viscous dominated region near no-slip walls, it is essential to use implicit algorithms which are not subject to stringent stability restrictions unrelated to accuracy requirements. Although it is possible to devise algorithms for solution of the governing equations as a fully coupled implicit system, such algorithms would require considerable iteration for the system of equations treated here, and this would detract from the overall efficiency. The present method is semi-implicit and seeks to reduce the amount of iteration required and yet avoid the more severe stability restrictions of explicit algorithms. The method partitions the system of equations into subsystems which govern the primary flow, the secondary flow and the turbulence model. The primary flow subset of equations contains the streamwise momentum equation. The secondary flow subset of equations contains the secondary vorticity equation and the scalar and vector potential equations. These subsystems are decoupled using an ad hoc linearization in which secondary velocity components and turbulent viscosity are lagged, and are solved sequentially during each axial step.

Summary of Algorithm

The governing equations are replaced by finite-difference approximations. Three-point central difference formulas are used for all transverse spatial derivatives. Analytical coordinate transformations are employed as a means of introducing a nonuniform grid in each transverse coordinate direction, as appropriate, to concentrate grid points in the wall boundary layer regions. Second-order accuracy for the transverse directions is rigorously maintained. Two-point backward difference approximations are used for streamwise derivatives, although this is not essential. To solve the primary flow subsystem of viscous equations for external flows, scalar ADI schemes are used for the streamwise momentum equation.

Given the solution for the primary flow, the secondary flow subsystem can be solved. First, the scalar potential equation (continuity) is solved using a scalar iterative ADI scheme. Next, the secondary vorticity and vector potential equations are written as a fully implicit coupled system and solved using an iterative linearized block implicit (LBI) scheme (cf. Briley and McDonald, Ref. 1). In selecting boundary conditions for the secondary flow subsystem, care must be taken to ensure that the final secondary velocity satisfies the no-slip condition accurately. Zero normal derivatives of ϕ are specified in the scalar potential equation, and this boundary condition corresponds to zero normal velocity. However, it is not possible to simultaneously specify the tangential velocity. Thus, the ϕ -contribution to the secondary velocity will have a nonzero tangential (slip) component, denoted v_t , at solid boundaries. In the coupled vorticity and vector-potential equations, both normal and tangential velocity components can be specified as boundary conditions, since these equations are solved as a coupled system. By choosing (a) zero normal velocity, and (b) $-v_t$ as the ψ -contribution to the tangential velocity, the slip velocity v_t arising from the ϕ calculation is cancelled, and the composite secondary flow velocity including both ϕ and ψ contributions will satisfy the no-slip condition exactly.

A summary of the overall algorithm used to advance the solution a single axial step follows. It is assumed that the solution is known at the n -level x^n and is desired at x^{n+1} .

- (1) The imposed streamwise pressure gradient distribution is determined from an a priori inviscid potential flow.
- (2) The streamwise momentum equation (10) is solved to determine u^{n+1} .
- (3) Using values now available for u^{n+1} , the scalar potential Eq. (8) is solved using an iterative scalar ADI scheme, to obtain ϕ^{n+1} . This ensures that the continuity equation is satisfied.
- (4) The equations for vorticity Eq. (14) and vector potential Eq. (9) form a coupled system for Ω^{n+1} and ψ^{n+1} which is solved as a coupled system using an iterative LBI scheme.
- (5) Values for the transverse velocities v_s and w_s are computed from Eq. (3).
- (6) Static pressure is computed from Eq. (13).

3. RESULTS

The initial effort, completed under the present program, has focused upon demonstrating the feasibility of computing the flow around submerged bodies at different attitudes by a forward marching computation procedure. Two test cases were identified for this demonstration. Laminar flow around a submerged yawed cylinder was considered as a first test case. This test case provided geometric simplicity while retaining important features of the flow around a submerged maneuvering body. The second test case considered high Reynolds number turbulent flow over a "tear-drop" shaped body at an angle of attack. The second test case was used to develop the capability to compute high Reynolds number turbulent flow fields over realistic body shapes using the forward marching procedure computer code (PEPSIG). Results of computations for the two test cases are presented in this section.

Laminar Flow over a Submerged Yawed Cylinder

Computed flows around a yawed cylinder at three yaw angles are presented in this section. Figure 1 shows a schematic of the configuration. The flow was assumed to be laminar at a Reynolds number of 10,000 based on the diameter of the cylinder. Computations were started on the cylinder with an assumed

streamwise velocity profile corresponding to an assumed initial boundary layer thickness. The initial boundary layer thickness for all the computations presented here was 10 per cent of the diameter of the cylinder. A transverse velocity field compatible with the assumed streamwise velocity field was computed at the initial station.

Figure 2 shows a vector plot of the secondary velocity field twenty cylinder diameters downstream of the initial station for three yaw angles: 5° , 10° and 15° . For purposes of clarity, only a part of the computational domain is shown in the figures. In all the cases the transverse flow rolls up into a vortex on the leeward side of the cylinder. This roll-up of the flow is caused by the transport of low momentum boundary layer fluid from the windward side around the cylinder to the leeward side. The low momentum fluid rolls up into a vortex on the leeward side of the cylinder. As would be expected, the strength of the vortex increases with yaw angle. Further, with the increase in yaw angle a smaller secondary vortex is formed close to the cylinder surface. The strength of this secondary vortex also increases with yaw angle.

Figure 3 shows a contour plot of the computed pressure field associated with the transverse velocity field shown in Fig. 2 for the three yaw angles. At the 5° yaw angle the transverse velocity field is weak and correspondingly causes no significant distortions of the transverse pressure field. At the 10° yaw angle, the primary vortex on the leeward side of the cylinder is sufficiently strong to cause a significant low pressure region to form at the vortex core. The pressure field associated with the primary vortex distorts the pressure field around the cylinder. At the 15° yaw angle, the increase in strength of the primary vortex decreases the pressure at the vortex core further and causes more significant distortions of the pressure field. Further, the secondary vortex closer to the leeward surface is sufficiently strong for additional low pressure pockets to form on the leeward side. The low pressure regions at high yaw angles could be a source of cavitation in the flow.

Turbulent Flow Over a "Tear-Drop" Shaped Body

Computation of high Reynolds number turbulent flow over a tear-drop shaped body at an angle of attack was used as a second test case. These computations were used to develop the capability of the forward marching procedure to compute high Reynolds number turbulent flow fields over realistic body shapes.

Geometry routines in the PEP SIG computer code have been modified to provide the capability to describe complex body shapes and generate a suitable computational grid. Figure 4 shows a tear-drop shaped body generated by the geometry routines. The body is axisymmetric with a NACA0025 thickness distribution. The geometry routines are also capable of handling elliptic cross-sections.

The flow field around a submerged tear-drop shaped body, shown in Fig. 4, at an angle of attack of 10° was computed using the forward marching procedure. Initially, to check capability to handle the body shape, laminar flow at a Reynolds number of 15000, based on the length (L) of the body, was computed. Since these results are qualitatively similar to the turbulent flow computations to be presented, for brevity the laminar flow computations are not shown here.

High Reynolds number turbulent flow over the tear-drop body at an angle of attack of 10° was also computed. The Reynolds number based on the length of the body was 1×10^6 . The computations were started on the body $0.02L$ downstream of the leading edge with an initial thin boundary layer (boundary layer thickness of $0.01L$). Crossflows compatible with the assumed streamwise velocity boundary layer profile at the starting station were computed with an iterative starting procedure. The final streamwise station of the computation was $0.98L$. Results of the computations at three streamwise stations ($x/L = 0.34, 0.66, 0.98$) are presented in this section. For purposes of clarity, only a part of the computational domain is shown in the figures that follow. The input streamwise pressure gradient was set to zero in the computations.

Figure 6 shows contours of the computed pressure field at the three streamwise stations. At $x/L = 0.34$, the pressure field contours show acceleration of the flow along the windward side followed by deceleration down the lee side. The adverse transverse pressure gradient causes the crossflow to separate on the lee side and begin to roll-up into a vortex. At $x/L = 0.66$, the pressure field associated with the rolled-up vortices forms two low pressure regions on the lee side. At $x/L = 0.98$, the vortices have moved away from the body showing a region of interaction between the low pressure vortex center and the body. This pressure field results in a sideward force on the body. Computed pressure perturbations are of the order of 5% to 10% of the freestream pressure.

Figure 7 shows a vector plot of the transverse velocity field at $x/L = 0.34$. The figure also shows close-ups of the transverse flow close to the

body surface. The lee side flow shows transverse flow reversal and the initial formation of a vortex. The windward side flow shows the thin boundary layers that need to be and have been resolved by the computations. Figure 8 shows the transverse velocity field at $x/L = 0.66$. The vortices on the lee side are clearly seen. A close-up of the flow near the body surface shows detail of the flow structure, the reversal of transverse velocity and the roll-up of the vortex. Figure 9 shows the transverse velocity field at $x/L = 0.98$, the final computation station. The flow field is dominated by the vortices on the lee side. A close-up of the flow field near the body surface reveals detail of the flow structure and the flow field resolved by the computation.

The computations presented demonstrate the capability of the forward marching procedure to compute high Reynolds number turbulent flow over submerged bodies at an angle of attack. The computations also demonstrate the capability to handle complex body shape and resolve the different length scales involved in the flow field. The present computations were carried out using 183,000 grid points (using half-plane symmetry) and required 520 seconds of computer time on a Cray. The computations are very economical considering the details of the flow field they provide.

4. CONCLUSIONS

The feasibility of computing the flow around a submerged body at different attitudes using the forward marching computation procedure has been demonstrated. Important features of the flow field have been captured in the computations. These features include the roll-up of the flow on the lee side into a pair of vortices. Distortion of the primary flow field and the pressure field by the vortices have been computed. Computations of the pressure field show low pressure regions at the center of the vortices. These low pressure regions could be a source of cavitation and noise. Computed pressure fields also show the effect of the vortices on the pressure field around the body. The capability to handle realistic body shapes and compute high Reynolds number turbulent flow fields has also been demonstrated. The computation procedure is very economical considering details of the flow field provided. All tasks proposed under this initial effort were successfully completed.

5. FUTURE WORK

Computation of the flow field over a submerged body using the forward marching procedure needs to be quantitatively verified by comparisons with available experimental data. Several tasks have been identified for this purpose and constitute current and future efforts under this program. These tasks would complete development of the forward marching procedure to compute flows over submerged bodies in maneuver.

REFERENCES

1. Briley, W.R. and McDonald, H.: Solution of the Multidimensional Compressible Navier-Stokes Equations by a Generalized Implicit Method. *Journal of Computational Physics*, Vol. 24, No. 4, 1977, p. 372.
2. Briley, W.R., McDonald, H. and Shamroth, S.J.: A Low Mach Number Euler Formulation and Application to Time-Iterative LBI Schemes, *AIAA Journal*, Vol. 21, Number 10, October 1983, pp. 1467-1469.
3. Liu, N.S., Shamroth, S.J. and Grubin, H.: Three-Dimensional Numerical Studies of the Physics of Semiconductor Crystal Growth, Scientific Research Associates, Inc., Report R82-920013-4, July 1982.
4. Briley, W.R. and McDonald, H.: Analysis and Computation of Subsonic Primary and Secondary Flows. *AIAA Paper 79-1453*, 1979.
5. Levy, R., Briley, W.R. and McDonald, H.: Viscous Primary/Secondary Flow Analysis for Use with Nonorthogonal Coordinate Systems. *AIAA Paper 83-0056*, 1983.
6. Kreskovsky, J.P., Briley, W.R. and McDonald, H.: Investigation of Mixing in a Turbofan Exhaust Duct, Part I: Analysis and Computational Procedure. *AIAA Journal*, Vol. 22, Number 3, March 1984.
7. Kreskovsky, J.P., Briley, W.R. and McDonald, H.: Analysis and Computation of Three-Dimensional Flow in Strongly Curved Ducts. Computers in Flow Predictions and Fluid Dynamics Experiments, ASME Winter Annual Meeting, 1981.
8. Shamroth, S.J. and Briley, W.R.: A Viscous Flow Analysis for the Tip Vortex Generation Process. *AIAA Paper 79-1546*, 1979.
9. Hull-Sail Interaction Flow Field, Contract Sponsored by the Naval Sea Systems Command General Hydrodynamics Research (GHR) Program under Contract N00014-84-C-0096.
10. Ship Propeller Tip Vortex Analysis, Contract Sponsored by The Office of Naval Research under Contract N00014-83-C-0768.

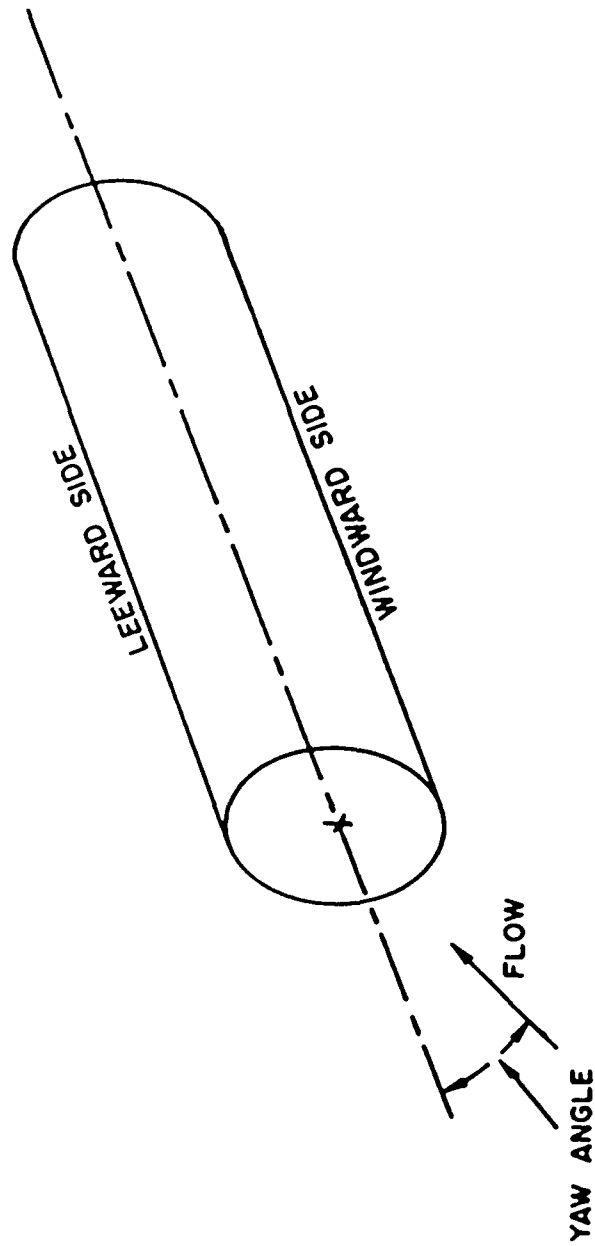
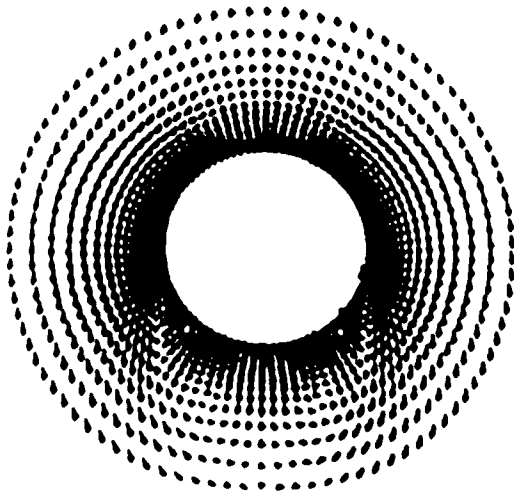
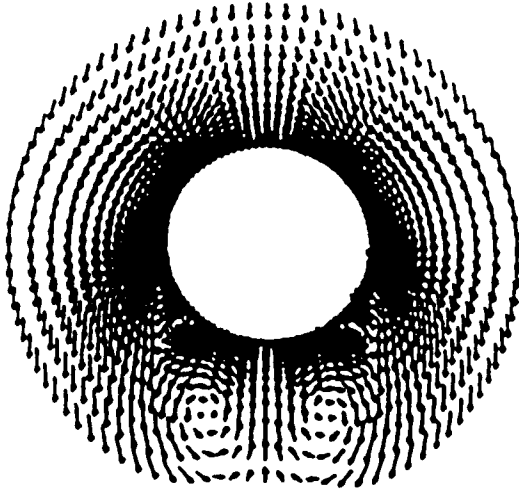


Figure 1. Schematic of the yawed cylinder

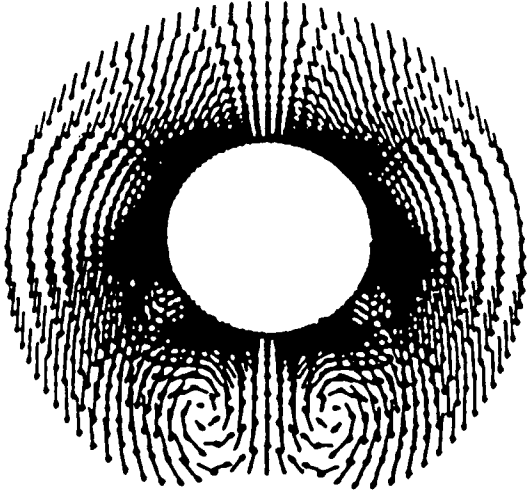
0.400



YAW = 5°



YAW = 10°



YAW = 15°

Figure 2. Transverse velocity vector plot

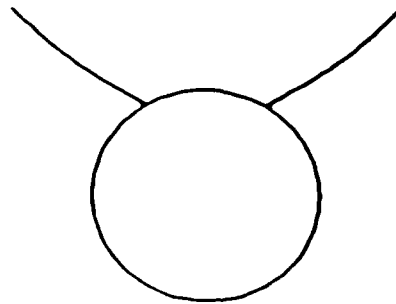
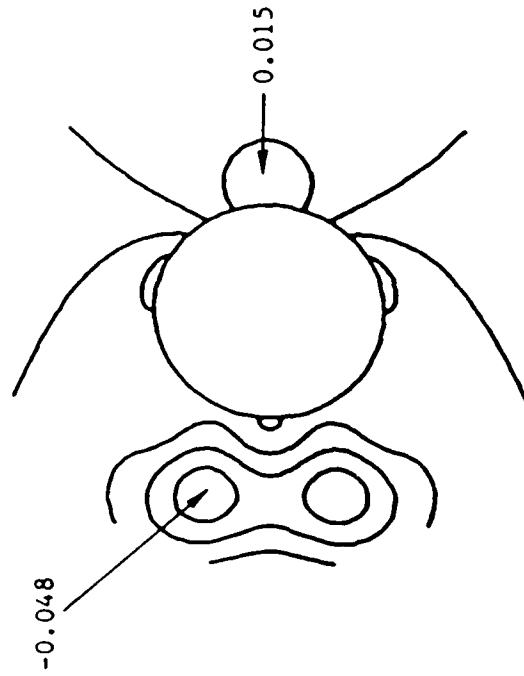
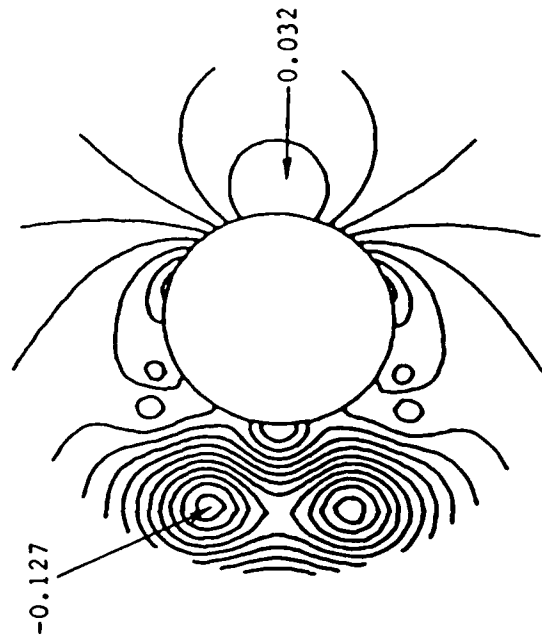


Figure 3. Pressure distribution contour plot

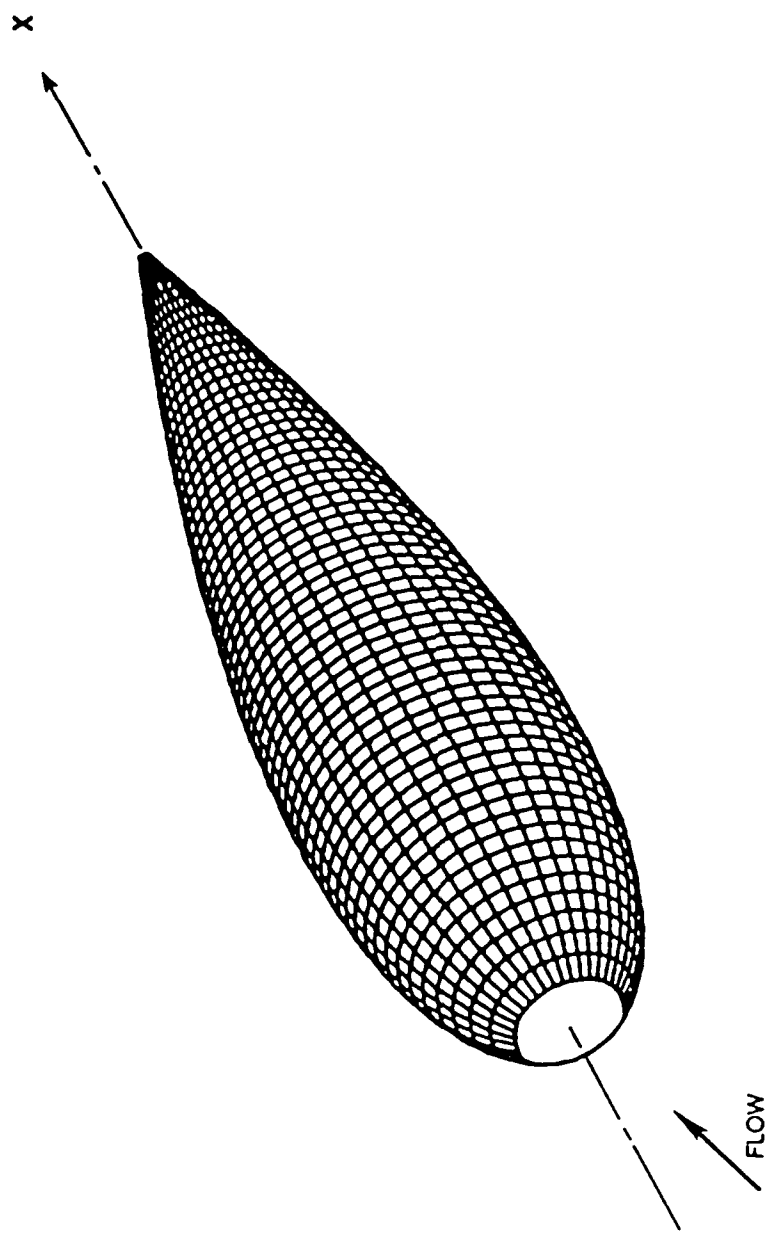
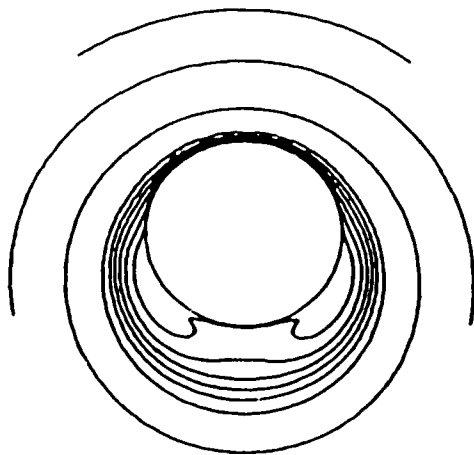
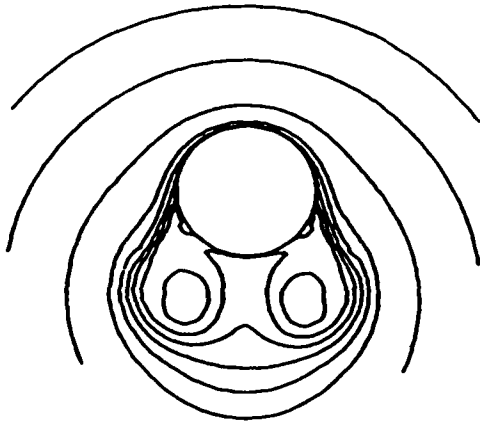


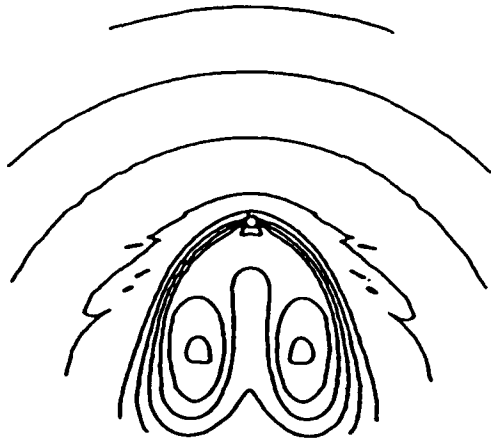
Figure 4. Perspective of "tear-drop" body



$x/l = 0.34$

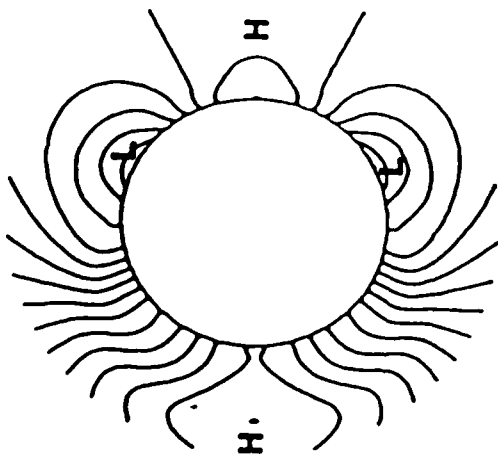


$x/l = 0.66$

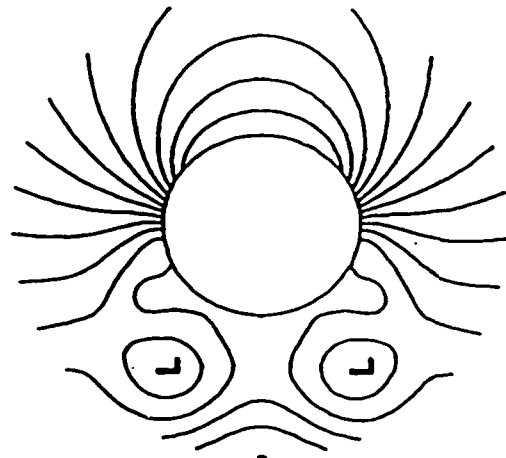


$x/l = 0.98$

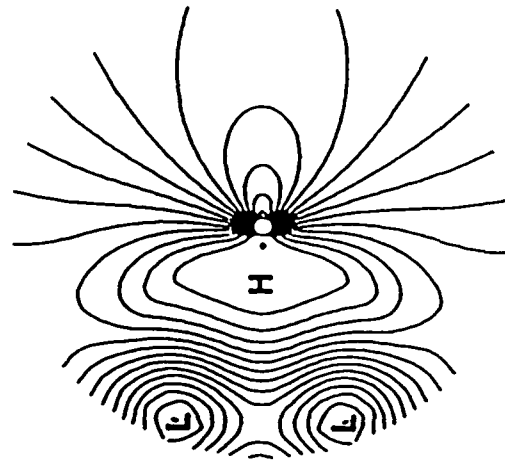
Figure 5. Streamwise velocity contours



$x/l = 0.34$



$x/l = 0.66$



$x/l = 0.98$

H - higher pressure regions
L - lower pressure regions

Figure 6. Computed pressure field contours

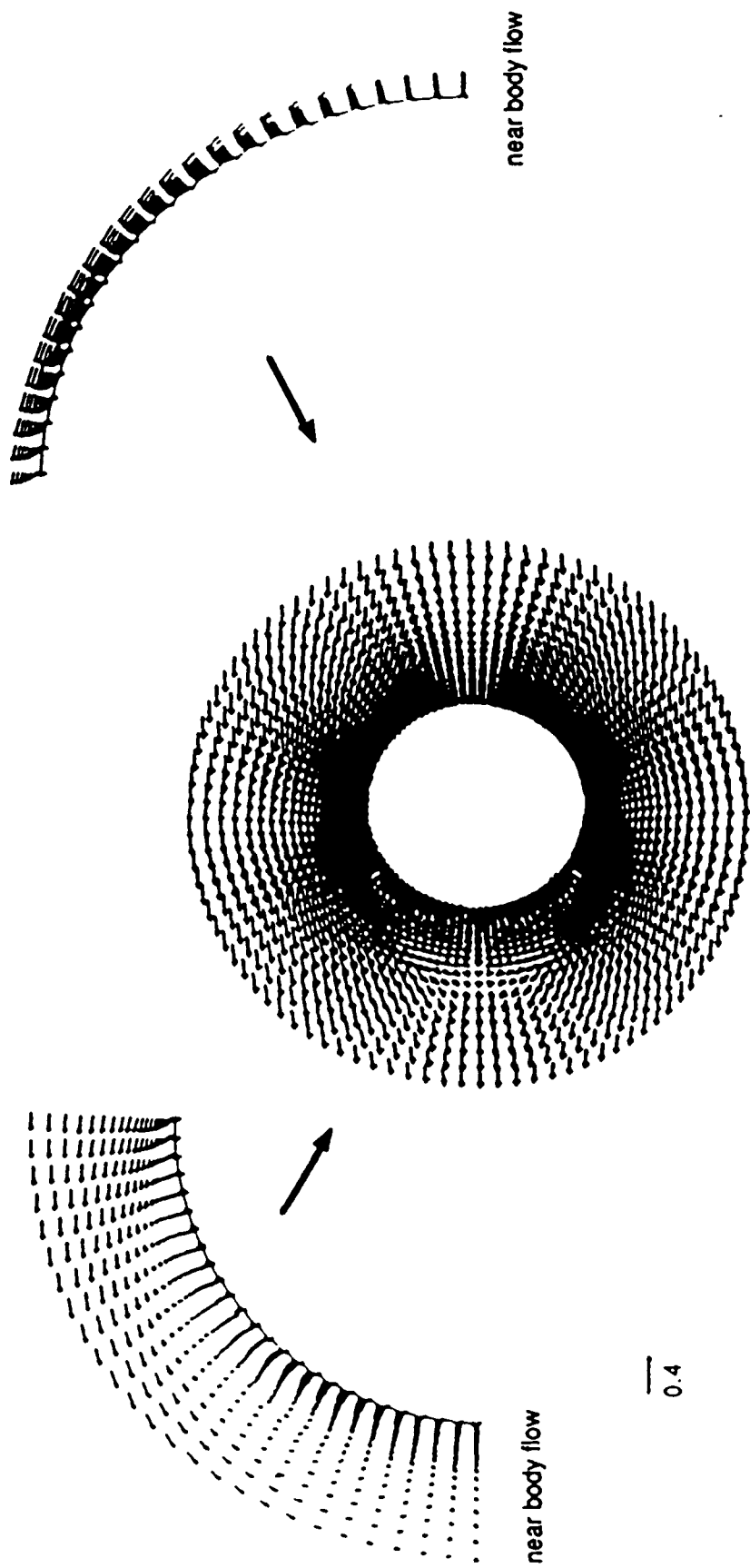


Figure 7. Transverse velocity field ($x/l=0.34$)

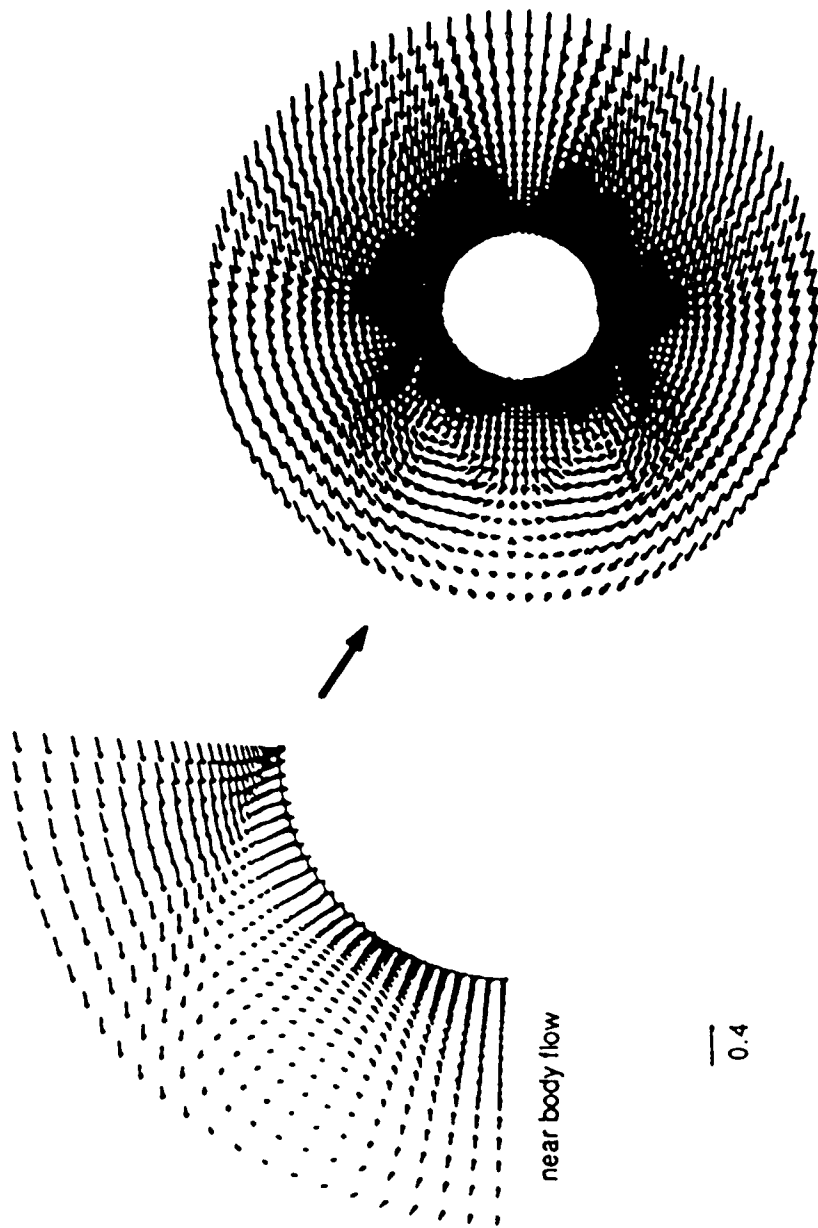


Figure 8. Transverse velocity field ($x/l=0.66$)

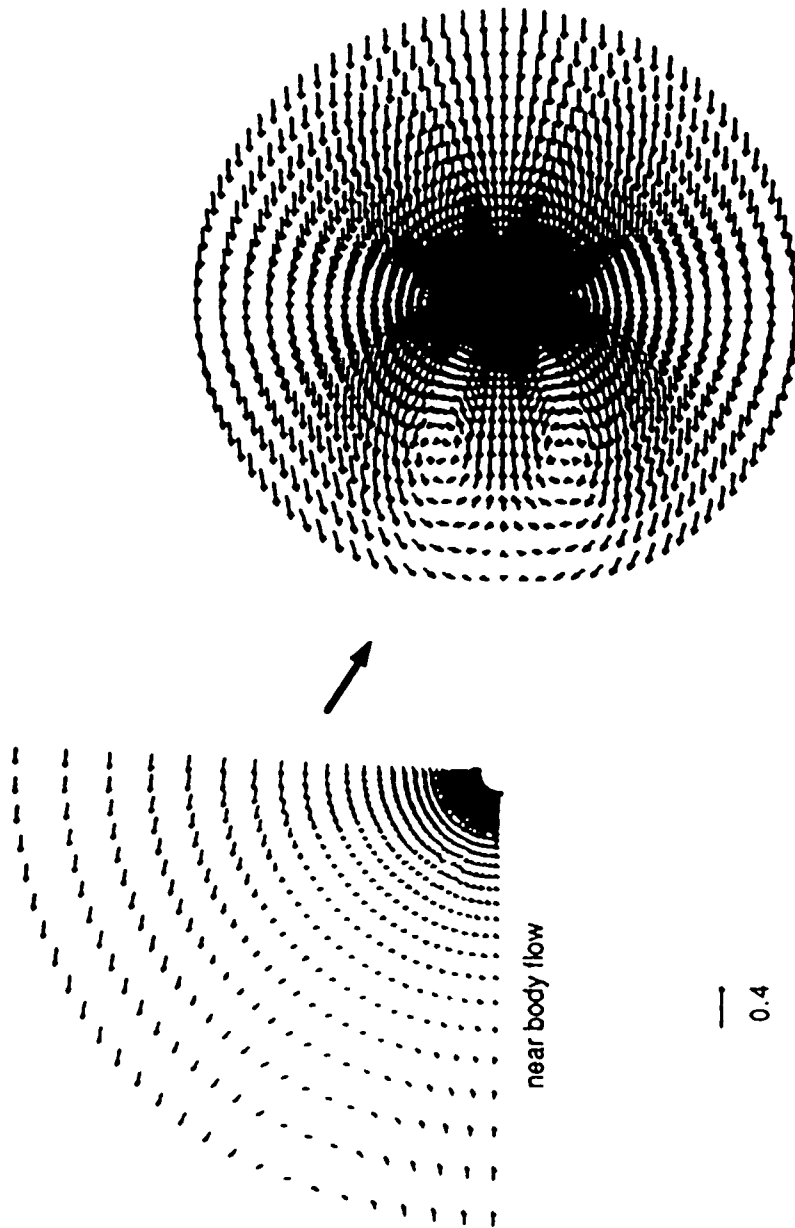


Figure 9. Transverse velocity field ($x/l = 0.98$)

END

9-87

Dtic